Shahrekord University

Journal of Microfluidic and Nanofluidic Research

Journal homepage: https://jmnr.sku.ac.ir

Research Article

Micromixing of Blood Plasma and DI water in a Passive Micromixer

Haneen Ahmed Sahib Al-Hachami, Morteza Bayareh*, Ahmad Reza Sajadi Dehkordi

Department of Mechanical Engineering, Shahrekord University, Shahrekord, Iran

ARTICLE INFO

Article history:

Received: 2025-02-18

Revised: 2025-03-15

Accepted: 2025-03-16

Keywords:

Microfluidics;

Micromixer;

Blood plasma;

DI water.

ABSTRACT

Micromixers are important devices in microfluidics designed for mixing liquids on a micro scale. These devices are crucial in chemistry, pharmaceuticals, analytical chemistry, biochemistry, and high-throughput synthesis due to their ability to manage small volumes of liquids with precision. In the present work, the mixing process in a converging-diverging micromixer is examined. The micromixer has three mixing units, each consisting of a chamber and an obstacle. For the reference case without an obstacle, molecular diffusion causes mixing at the interface of the two fluids, and with an increase in the number of mixing units and fluid advancement, the effect of molecular diffusion becomes more pronounced. It is also observed that with an increase in input velocity, the mixing index also increases. In the first case, the formation of vortices behind the obstacle leads to greater mixing of the two liquids. Compared to the reference case, the mixing index of the first case increases from 19.12% to 30.21% at an inlet velocity of 0.001 m/s. In the second case, unlike the first one, the maximum mixing index occurs at the lowest inlet velocity. The mixing index for the first and third cases is 34.26% and 56.24%, respectively. However, the pressure drop also increases from 48220 Pa to 58807 Pa. In the fourth case, square obstacles do not significantly increase efficiency, and its efficiency is higher than that of the reference case and lower than that of the other cases.

1. Introduction

Microfluidics is a field that manipulates microscopic amounts of liquids within channels, typically ranging from 1 to 1000 micrometers, and due to their small scale, they offer precise control and unique behavior of fluids. This technology integrates complex laboratory operations into small and simple systems, resulting in reduced sample consumption, faster reaction times, and higher accuracy. The ability to control chemicals, cells, or enzymes with great precision has made microfluidics a revolutionary tool in various scientific and industrial fields [1]. These devices can be divided into two main types: passive micromixers that work based on the geometry of microchannels to improve mixing through diffusion and chaotic flow patterns, and active micromixers that use external energy sources such as electric or magnetic fields to enhance mixing [2-4].

Chen and Zhao [5] focused on the optimal design of obstacle arrangements in a three-dimensional T-shaped micromixer. Numerical analysis showed that the flow direction continuously changes due to the presence of obstacles, leading to chaotic displacement and significantly enhanced mixing of two liquids. The weight of the influencing parameters, in order, was: obstacle height > geometric shape >

* **Corresponding author.**
E-mail address: m.bayareh@sku.ac.ir

Cite this article as:
Alhachami, H., Bayareh, M., and Sajadi, AR., 2025. Micromixing of Blood Plasma and DI water in a Passive Micromixer. *Journal of Microfluidic and Nanofluidic Research*, 2(1), pp. 48-54.
https://doi.org/10.22034/jmnr.2025.15162.1006

symmetry = number of obstacles. Based on the optimized results, a new micromixer was designed. Compared to the T-shaped micromixer, the micromixer with obstacles was more efficient, achieving a mixing index of over 90 percent across a wide range of Péclet numbers. They demonstrated that the proposed optimal design method for obstacle arrangement in three-dimensional microchannels is a simple and effective technology for improving mixing in microfluidic devices.

Shouman et al. [6] presented a new planar micromixer inspired by hepatic sinusoids and examined the effects of geometric parameter variations on its performance. The micromixer was constructed from polydimethylsiloxane using photolithography, and experiments were conducted to validate the computational model. An improved micromixer design was achieved, suitable for laminar flow. The results demonstrated promising performance within the studied Reynolds and Péclet number ranges, particularly at low Reynolds numbers. A mixing index of up to 99 percent was achieved with a pressure drop of less than 5000 pascals.

An inactive micromixer based on the concept of a three-dimensional helical microchannel for dividing and recombining flow using OH-shaped sections was developed by Hossein and Kim [7]. The flow and mixing performance were numerically analyzed using the Navier-Stokes equations and mass conservation with a dispersion-diffusion model over a Reynolds number range of 0.01 to 120. The results showed that dividing and recombining flow in the helical micromixer design improved mixing performance within the tested Reynolds number range, and the proposed micromixer achieved a mixing index of 0.884 at a Reynolds number of 30.

Chen et al. [8] designed a micromixer based on a tree-like fractal structure. The goal was to achieve a micromixer with better mixing performance by altering the structure. They concluded that the micromixer with a fractal dimension of 2 and a 90-degree angle at each Reynolds number had a high mixing index. The fractal dimension had the most significant impact on the micromixer's structure, and the mixing performance of the micromixers improved with an increase in the fractal dimension.

Several new micromixers based on Baker's theory with continuous layering according to the chaotic advection theory were designed by Ruijin et al. [9]. To demonstrate the complete mixing index and mixing mechanism in this micromixer, numerical simulations were conducted, and comparisons were made with other micromixers that divide and recombine flow. The numerical results showed that this micromixer has a better mixing index at low Reynolds numbers, attributed to the presence of more interfacial surfaces between the two flows due to the layering effect. Additionally, the presence of curved channels could create secondary flow and help improve mixing. Chen and Chen [10] designed a structure based on the topology optimization method. This structure allowed two fluids to experience reverse flow and enhanced chaotic displacement. This research considered the circular structure as the main structure and analyzed topological micromixers with circular structures through numerical simulation. Their mixing index and pressure drop were analyzed with different Reynolds numbers.

Another type of passive micromixer is the converging-diverging type. This structure generates expansion vortices, disrupts the interface between two liquids, and increases their contact surface area. Thus, it improves the mixing index. For example, Afzal and Kim [11] proposed a converging-diverging micromixer with a T-shaped inlet. Afzal and Kim [12] also used flow splitting and recombination in conjunction with the converging-diverging structure and showed that the mixing index reaches 95% with an increase in the Reynolds number from 10 to 70.

In the present work, a converging-diverging micromixer is designed so that, in addition to the expansion and contraction features, expansion vortices are also formed in the micromixer, which significantly enhance the mixing index. The micromixer has three mixing units, each consisting of a chamber and an obstacle (Fig. 1).

2. Governing Equations

Considering the following assumptions

1- Fluids are incompressible.

2- Fluids exhibit Newtonian behavior.

3- The simulations are conducted in a steady state.

4- The geometry of the micromixer is two-dimensional.

5- The thermophysical properties of the two fluids are different.

The governing equations (continuity and momentum) in the steady state for the mixing of two fluids are expressed as follows:

$$\nabla \cdot \vec{V} = 0 \quad (1)$$

$$\rho \vec{V} \cdot \nabla \vec{V} = -\nabla P + \mu \nabla^2 \vec{V} \quad (2)$$

where $\vec{V}$ is the velocity vector, P is the pressure, ρ is the density, and μ is the dynamic viscosity. The convective-diffusion transport equation for species i is also introduced as follows:

$$\vec{V} \cdot \nabla C_i = D_i \nabla^2 C_i \quad (3)$$

which C_i indicates concentration and D_i is molecular diffusion. Additionally, the mixing index is calculated as follows:

$$MI = \left(1 - \left(\sqrt{\frac{1}{N}\sum_{i=1}^{N}\left(\frac{c_i - \bar{c}}{\bar{c}}\right)^2}\right)\right) \times 100 \quad (4)$$

In this equation, c_i is the local concentration of each component and $\bar{c}$ is the average concentration. N also represents the number of grid points in the desired cross-section.

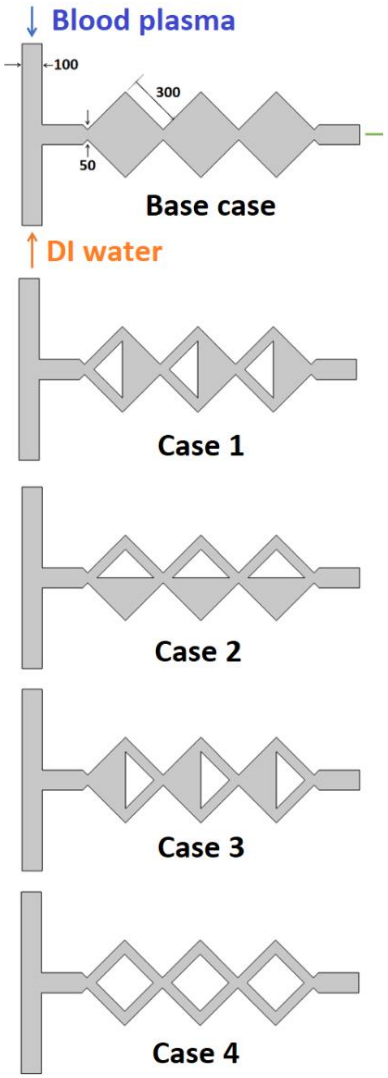

Fig. 1. Schematic of the proposed micromixers. The dimensions are in micrometers.

3. Grid Study and Validation

In this section, an example of the steps to examine the independence of the solution from the computational grid for the base case is presented. Four grids with 25784, 50048, 104751, and 156751 elements were generated, and the velocity distribution was calculated at a section before the first mixing unit. Fig. 2 shows the velocity distribution in this section. This figure indicates that the grids with 104751 and 156751 computational elements yield very similar results. Therefore, the grid with the lower computational cost, namely the grid with 104751 elements, is chosen for the simulations. The representation of this computational grid is shown in Fig. 3.

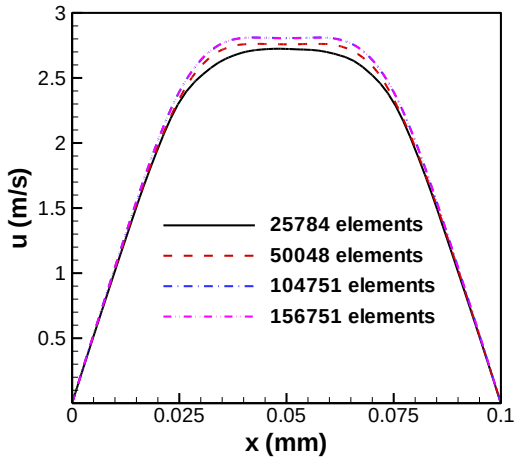

Fig. 2. Velocity distribution in a cross-section before the first mixing chamber with different computational grids.

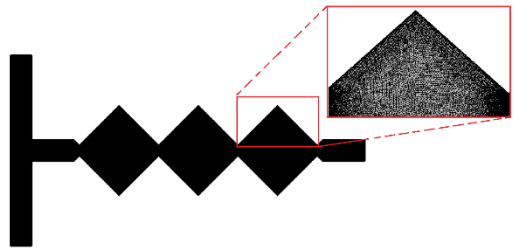

Fig. 3. The computational grid generated for the base case.

For the validation, the numerical results of Afzal and Kim [12] are used. They investigated three passive micromixers with converging-diverging channel walls with sinusoidal variations. The mixing of water and ethanol was conducted in the Reynolds number range of 10 to 70. Their results indicated that the mixing performance is significantly dependent on the throat width. However, the mixing performance was not sensitive to the wall diameter in the selected Reynolds number range. The mixing efficiency values obtained from the present work and Afzal and Kim [12] are compared in Table 1. This table indicates a good agreement between the results; therefore, the numerical solution method in the present work can be used for simulations.

Table 1. Values of MI for different amounts of Re.

Re	Present work	Afzal and Kim [12]
10	0.3742	0.3625
20	0.5711	0.5542
30	0.7613	0.7417
40	0.8602	0.8416

4. Results

Fig. 4 shows the concentration contour along the base micromixer at different inlet velocities. Molecular diffusion is the dominant mixing mechanism at low inlet velocities in the micromixer. Therefore, the role of molecular diffusion in passive micromixers, where laminar flow predominates, is much greater because there is no chaotic flow, making the process inherently slow as molecules move along concentration gradients. This limitation becomes prominent in applications requiring rapid mixing, such as chemical reactions or biological assays. The effect of molecular diffusion is more pronounced for low flow rate applications, but it decreases at higher flow rates, necessitating a balance between mixing efficiency and pressure drop in micromixer design.

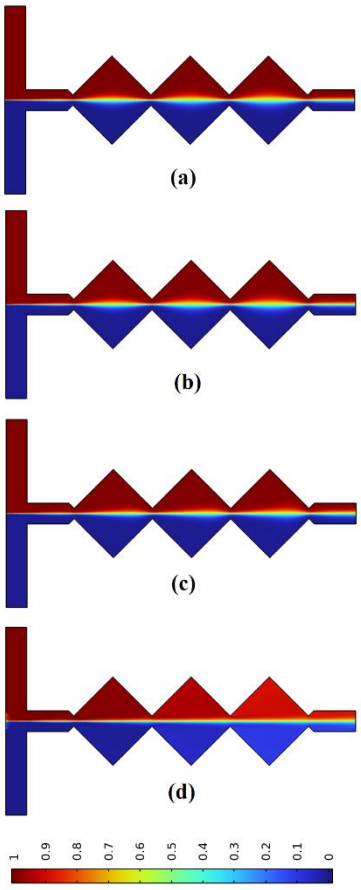

Fig. 4. Concentration contour along the base case for different inlet velocities: (a) 0.001 m/s, (b) 0.01 m/s, (c) 0.1 m/s, and (d) 1 m/s.

Fig. 4 shows that molecular diffusion causes mixing at the interface of two fluids, and its effectiveness becomes more apparent with an increase in the number of mixing units and fluid advancement. Additionally, it is observed that the mixing efficiency increases with higher inlet velocities. Table 2 confirms this observation. Furthermore, the pressure drop results indicate that the pressure drop increases with higher inlet velocities. Specifically, as the inlet velocity increases from 0.001 to 1 meter per second, the pressure drop rises from 4.85 to 18900 pascals, highlighting the significant impact of inlet velocity on this parameter.

Table 2. Mixing efficiency and pressure drop values of the base case for different inlet velocities.

U_{in} (m/s)	Δp (Pa)	MI (%)
0.001	4.85	19.12
0.01	48.85	19.72
0.1	612.93	22.76
1	18900	39.76

In Case 1, the triangular barrier causes the flow to split and then merge in each mixing chamber. The formation of vortices behind the barrier leads to greater mixing of the two liquids. Fig. 5 confirms this. This figure indicates that with an increase in inlet velocity, the mixing efficiency also increases. Here, the occurrence of larger vortices behind the barrier is the main reason for the increase in efficiency. Table 3 quantitatively shows the results related to mixing efficiency and pressure drop. Compared to the baseline case, the mixing efficiency at a velocity of 0.001 m/s increases from 19.12 to 30.21. Additionally, the pressure drop at this inlet velocity increases from 4.85 Pascal in the baseline case to 12.75 Pascal in this case. It is observed that as the inlet velocity increases, the percentage increase in mixing efficiency and, correspondingly, the percentage increase in pressure drop also become greater.

In Case 2, the triangular obstacles are positioned such that the base of the triangle is aligned with the flow direction. In other words, a portion of the fluid (blood plasma) is drawn down the chamber, which increases the mixing efficiency compared to the baseline condition. However, it is noteworthy that the highest mixing efficiency occurs at a lower inlet velocity. In fact, a larger fraction of the blood plasma is driven down the chamber at lower velocities, leading to an even greater increase in mixing efficiency. Fig. 6 clearly shows that increasing the inlet velocity up to 1 meter per second significantly reduces the volume of blood plasma that separates from the upper section. Table 4 also confirms this observation. Unlike the first case, the maximum mixing efficiency occurs at the lowest inlet velocity. Since the pressure drop at this velocity is very low, this condition can be considered an optimal state for the micromixer's efficiency.

In Case 3, the triangular obstacles are positioned in such a way in the mixing chambers that the base of the triangle is perpendicular to the flow direction, causing the flow to split. Fig. 7

shows that the placement of the triangular obstacle in this manner has significantly increased the mixing efficiency. Similar to the base case and the first case, here too, the mixing efficiency increases with the increase in inlet velocity, but the percentage increase compared to the base case and the first case is much higher (Table 5).

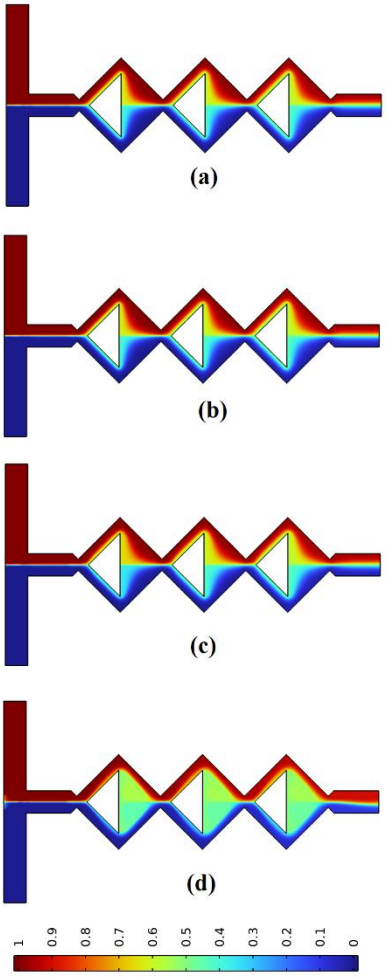

Fig. 5. Concentration contour along Case 1 for different inlet velocities: (a) 0.001 m/s, (b) 0.01 m/s, (c) 0.1 m/s, and (d) 1 m/s.

Table 3. Mixing efficiency and pressure drop values of Case 1 for different inlet velocities.

U_{in} (m/s)	Δp (Pa)	MI (%)
0.001	12.75	30.21
0.01	127.93	31.48
0.1	1431.3	31.93
1	48220	34.26

For example, at a velocity of 1 meter per second, the mixing efficiency for the first and third cases is 34.26% and 56.24%, respectively. However, the pressure drop also increases from 48,220 pascals to 58,807 pascals. In this case, when the two liquids collide at the base of the triangle, a stagnation point is formed, and two vortices are created at the point of collision. At low velocities, these vortices increase the mixing efficiency. However, as the inlet flow velocity increases, the size of these vortices decreases, but the flow that meets after the obstacles has a higher velocity, causing flow separation at the sharp edges of the triangular obstacles. In fact, the significant increase at higher velocities is due to the formation of vortices at the two edges of the triangular obstacles.

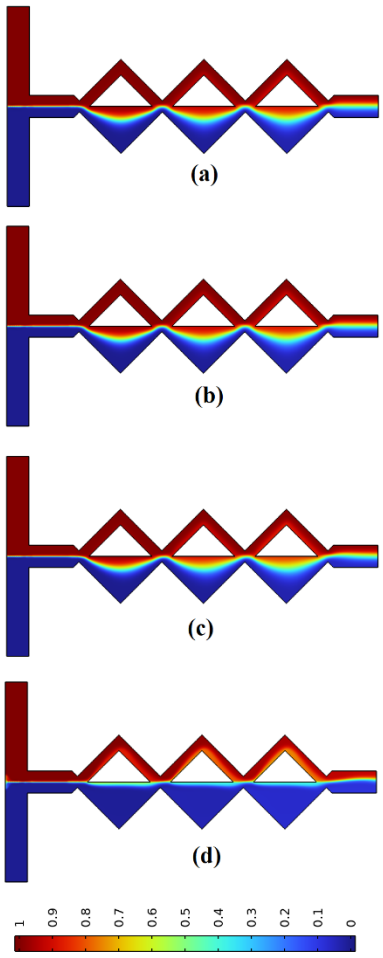

Fig. 6. Concentration contour along Case 2 for different inlet velocities: (a) 0.001 m/s, (b) 0.01 m/s, (c) 0.1 m/s, and (d) 1 m/s.

Table 4. Mixing efficiency and pressure drop values of Case 2 for different inlet velocities.

U_{in} (m/s)	Δp (Pa)	MI (%)
0.001	8.71	34.09
0.01	87.53	33.5
0.1	1031.2	33.6
1	42626	30.66

In Case 4, the obstacles within the chambers are arranged in a way that they form squares. The flow of the two liquids separates upon encountering the square obstacles and rejoins after passing through them. Fig. 8 shows that the square obstacles do not significantly increase the efficiency, and among the studied cases, only its efficiency is higher than the baseline. This

figure indicates that no vortices are formed under these flow conditions, and increasing the inlet velocity only pushes a larger portion of each fluid into the passage between the chambers and obstacles, thereby slightly increasing the efficiency. Table 6 also confirms this, showing that in this case, the pressure drop also increases with the increase in velocity.

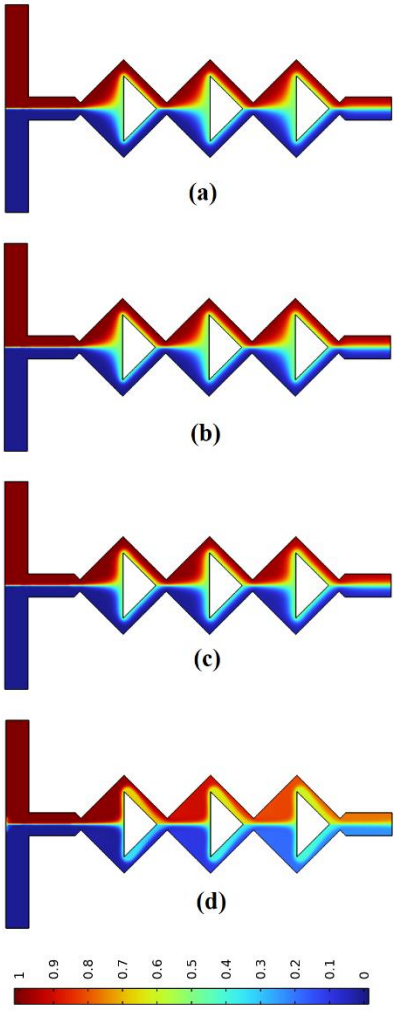

Fig. 7. Concentration contour along Case 3 for different inlet velocities: (a) 0.001 m/s, (b) 0.01 m/s, (c) 0.1 m/s, and (d) 1 m/s.

Table 5. Mixing efficiency and pressure drop values of Case 3 for different inlet velocities.

U_{in} (m/s)	Δp (Pa)	MI (%)
0.001	12.78	31.16
0.01	128.24	32.60
0.1	1456.4	35.37
1	58807	56.24

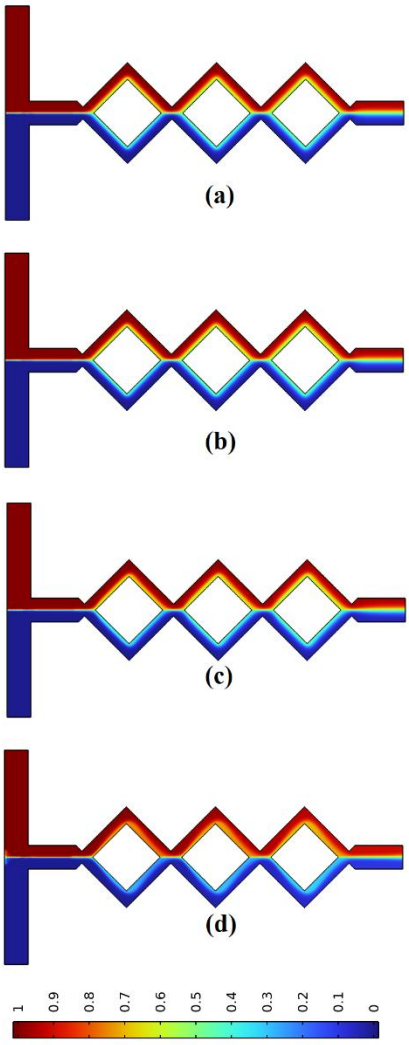

Fig. 8. Concentration contour along Case 4 for different inlet velocities: (a) 0.001 m/s, (b) 0.01 m/s, (c) 0.1 m/s, and (d) 1 m/s.

Table 6. Mixing efficiency and pressure drop values of Case 4 for different inlet velocities.

U_{in} (m/s)	Δp (Pa)	MI (%)
0.001	17.22	29.86
0.01	172.58	30.56
0.1	1856.3	31.29
1	47374	32.49

5. Conclusions

The mixing process in a converging-diverging micromixer is investigated in this paper. Each of the three mixing units in the micromixer is made up of an impediment and a chamber. Molecular diffusion results in mixing at the interface between the two fluids in the reference case without an obstruction. The effect of molecular diffusion intensifies as the number of mixing units and fluid advancement increases. Additionally, it has been noted that the mixing

index rises in tandem with an increase in input velocity. In the first instance, the two liquids mix more because of the vortices that form behind the obstruction. At an input velocity of 0.001 m/s, the first instance's mixing index rises from 19.12% to 30.21% in comparison to the reference case.

References

[1] Bayareh, M., Nazemi Ashani, M., Usefian, A., 2020. Active and passive micromixers: A comprehensive review, Chem. Eng. Process.: Process Intensif., 147, p. 10777. https://doi.org/10.1016/j.cep.2019.107771

[2] Ghorbani Kharaji, Z., Bayareh, M., Kalantar, V., 2021. A review on acoustic field-driven micromixers, Int. J. Chem. React. Eng., 19, pp. 553-569. https://doi.org/10.1515/ijcre-2020-0188.

[3] Bayareh, M., 2022. Active cell capturing for organ-on-a-chip systems: a review, Biomedical Engineering, 67, pp. 443-459. 10.1515/bmt-2022-0232.

[4] Jafari Ghahfarokhi, N., Bayareh, M., Nourbakhsh, A., Baghoolizadeh, M., 2024. Optimization of a novel micromixer with fan-shaped obstacles, Chem. Pap., 78, pp. 4201-4210. https://doi.org/10.1007/s11696-024-03380-y.

[5] Chen, X., Zhao, Z., 2017. Numerical investigation on layout optimization of obstacles in a three-dimensional passive micromixer, Analytica Chimica Acta, 964, pp. 142–149.

[6] Shouman, M.A., El-Shazly, A.H., Elkady, M.F., Salem, M.S., Elmarghany, M.R., Sabry, M.N., 2019. Shape Optimization of an Innovative Hepatic Sinusoids-Based Micromixer, Chemical Engineering and Processing - Process Intensification, 146, p. 107684.

[7] Hossain, S., Kim, K.-Y., 2015. Mixing analysis in a three-dimensional serpentine split-and-recombine micromixer, Chemical Engineering Research and Design, 100, pp. 95–103.

[8] Chen, Y., Chen, X., Liu, S., 2020. Numerical and experimental investigations of novel passive micromixers with fractal-like tree structures, Chemical Physics Letters, 747, pp. 137330.

[9] Ruijin, W., Beiqi, L., Dongdong, S., Zefei, Z., 2017. Investigation on the splitting-merging passive micromixer based on Baker's transformation, Sensors and Actuators B: Chemical, 249, pp. 395–404.

[10] Chen, Y., Chen, X., 2019. An improved design for passive micromixer based on topology optimization method, Chemical Physics Letters, 734, pp. 136706.

[11] Afzal, A., Kim, K.Y., 2012. Passive split and recombination micromixer with convergent-divergent walls, Chemical Engineering Journal, 203, pp. 182-192.

[12] Afzal, A., Kim, K.Y., 2015. Convergent-divergent micromixer coupled with pulsatile flow, Sensors and Actuators, B: Chemical, 211, pp. 198-205.